



Magnetic frustration and fractionalization in oligo(indenoindenes)Ricardo Ortiz ¹, Geza Giedke,^{1,2} and Thomas Frederiksen ^{1,2}¹*Donostia International Physics Center (DIPC), E-20018 San Sebastián, Spain*²*IKERBASQUE, Basque Foundation for Science, E-48013, Bilbao, Spain* (Received 30 November 2022; revised 24 February 2023; accepted 13 March 2023; published 27 March 2023)

Oligo(indenoindenes) (OInIn) are π -conjugated ladder carbon polymers with alternating hexagons and pentagons, hosting one unpaired electron for each of the latter in the open-shell limit. Here we study the main magnetic interactions in finite OInIn, classifying the six possible isomers in two different classes of three isomers each. We find that one class can be described by frustrated $S = 1/2$ Heisenberg chains, with antiferromagnetic interactions between the second-neighbor sites. The other class is characterized by antiferromagnetic order. Employing several levels of theory, we further show that the ground state of one of the isomers is a valence-bond solid of ferromagnetic dimers ($S = 1$). This is topologically similar to that of the Affleck-Kennedy-Lieb-Tasaki (AKLT) model, which is known to show fractional $S = 1/2$ states at the edges.

DOI: [10.1103/PhysRevB.107.L100416](https://doi.org/10.1103/PhysRevB.107.L100416)

Introduction. The study of graphene-related systems as a playground for realizing exotic phases of matter is a topic of intense research in modern physics. The observation of superconductivity in magic-angle twisted bilayer graphene [1], or the discovery of fractional edge states in triangulene chains [2], would be fair examples of such a claim. Thus, as a generalization of the latter, open-shell nanographenes that host localized electrons can be used to design more complex architectures that mimic model and spin Hamiltonians, displaying the nontrivial physics of these models [2–12].

Inconveniently, the high reactivity inherent to unpaired electrons has prevented the realization of these systems for many decades. Solely recent experiments employing on-surface synthesis in ultra-high-vacuum conditions has shown to be effective for obtaining such pristine open-shell molecules [13–16]. Further characterization, by means of scanning tunneling microscopy, has also probed the existence of local moments by measuring Kondo peaks [17–19] or inelastic steps [20–22]. Today this is a well-established technology, so there is a plethora of platforms with localized electrons and π magnetism [23,24].

Electron localization in nanographenes is related very often with states pinned at (or close to) the Fermi energy [25], which can originate from several sources such as sublattice imbalance [26] or nontrivial topology [27,28]. These zero modes can interact by different exchange mechanisms [29,30], leading to either ferromagnetism or antiferromagnetism. For bipartite lattices, the total spin quantum number of the ground state at half-filling can be predicted by Lieb's theorem [31] $S = |N_A - N_B|/2$ (with $N_{A,B}$ sites belonging to the sublattices A and B), which was originally formulated for the Hubbard model and later found to be in agreement with numerical results beyond this model [32].

In the following we will focus on nonbipartite systems, more specifically, finite conjugated ladder polymers that alternate hexagons and pentagons: the oligo(indenoindenes) (OInIn, Fig. 1). The inclusion of P pentagons induces

frustration in the sublattices [33], making Lieb's theorem no longer applicable, but one may expect exchange interactions to work similar to those in bipartite lattices. For instance, two overlapping electrons show ferromagnetic (FM) exchange [29,30] ($J^{\text{FM}} \propto U$), while coupling through hopping leads to kinetic antiferromagnetic (AF) exchange [30,34,35] ($J^{\text{AF}} \propto 1/U$). It is worth mentioning that there might be other interactions that can be important, i.e., Coulomb-driven exchange [29,30], but the former two will play the dominant role in the systems discussed here.

In Fig. 1 we show the six possible isomers that can be drawn by keeping invariant the angle of two vectors that point in the vertex direction of adjacent pentagons. Despite their high instability, experiments on several of these systems have been reported, like the antiaromatic $P = 2$ island [36] and oligomers [37] of isomer 4. In the latter case, it is expected by theory [38,39], and confirmed by atomic force microscopy experiments [36], that the shortest island is closed shell, but calculations indicate that the ground state develops magnetism if the system is enlarged [37,40,41]. The synthesis of a C_3 symmetric derivative (truxene-5,10,15-triyl) with $S = 3/2$ ground state is also confirmed [42,43], as well as polymers of $P = 2$ islands [44] of isomer 2, and polymers of $P = 2$ islands of isomer 4 with intercalations [45] of isomer 5.

Drawing the maximum number of Clar sextets in OInIn leaves one unpaired electron per pentagon [46], justifying their radical character. According to this, we argue that such indenofluorene derivatives, with P pentagons and $P + 1$ hexagons, may be understood as effective electron chains with P sites. This picture corresponds to the open-shell limit and it is convenient for our purpose in this Letter, although a more realistic description would consist of a combination of different configurations that reduces the radical character [47]. This is of special relevance for some $P = 2$ islands that are closed shell [38,39], but simplifying the system to electron chains allows us to study the exchange mechanisms at a fundamental level, which also explains the physics of the shortest molecules.

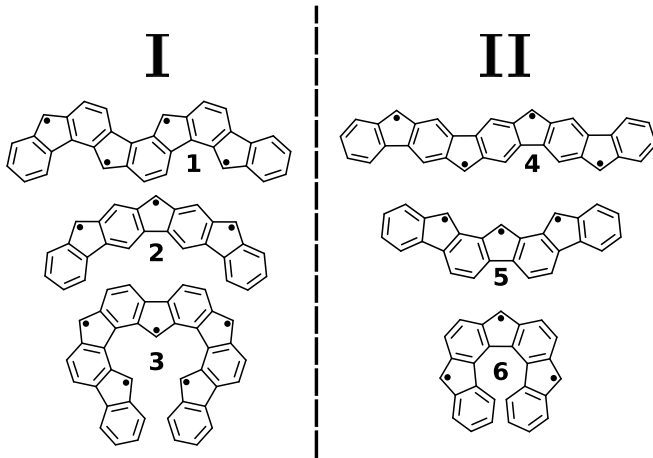


FIG. 1. Isomeric forms of OInIn in the open-shell configuration. Any other isomeric system is just a combination of these. According to our analysis, the structures can be grouped into classes I and II according to different magnetic interactions.

Thus, in this Letter two things are done. First, we consider that the OInIn can be interpreted, in the tight-binding (TB) approximation, as bipartite systems plus a hopping t' that closes the pentagons [48]. Then, when interactions are considered, we show that isomer 1 in the vicinity of $t' = t$ has a ground state that consists in $P/2$ FM dimers with effective $S = 1$ quantum number each [Fig. 2(a)]. Second, in order to explain these results, we perform an analysis of the different magnetic exchanges. By this we manage to classify the six isomers in two different groups: antiferromagnets (isomers 4, 5 and 6) and frustrated chains with antiferromagnetic second-neighbor interactions (isomers 1, 2, and 3).

Methods. We consider electron interactions by means of the Hubbard model, that we solve using two approaches: a collinear mean-field (MF) approximation and an exact diagonalization with a complete active space CAS(N_e, N_o), where N_e (N_o) refers to the number of electrons (single-particle orbitals) included, and $t = -2.7$ eV. For nanographenes and related structures, usually all the hoppings are chosen similar ($t' \approx t$) and the on-site repulsion inside a certain range [49] ($|t| < U < 2.2|t|$), but we present some results as a function of t' and U in order to check the stability of the proposed ground state and also to contrast with the physical behavior of the effective spin models. Then we compare the results of isomer 1 with those from density functional theory (DFT), where we employed QuantumESPRESSO (QE) [50–52] with the Perdew-Burke-Ernzerhof (PBE) [53] exchange-correlation functional as well as ORCA [54] with the PBE0 hybrid functional [55,56] (details in Sec. S1) [57].

Results. The origin of magnetism in the OInIn lies in the unpaired electrons, which are mainly localized at the pentagons. These can be visualized in a simple noninteracting TB approximation ($U = 0$), where P single-particle states are present inside a big gap in isomer 1 [Fig. 2(b)]. Such in-gap states can be understood as the hybridized zero modes of the bipartite molecule with $t' = 0$ and sublattice imbalance $|N_A - N_B| = P$. Apparently, this hybridization is not enough to quench magnetism, and local moments appear in a

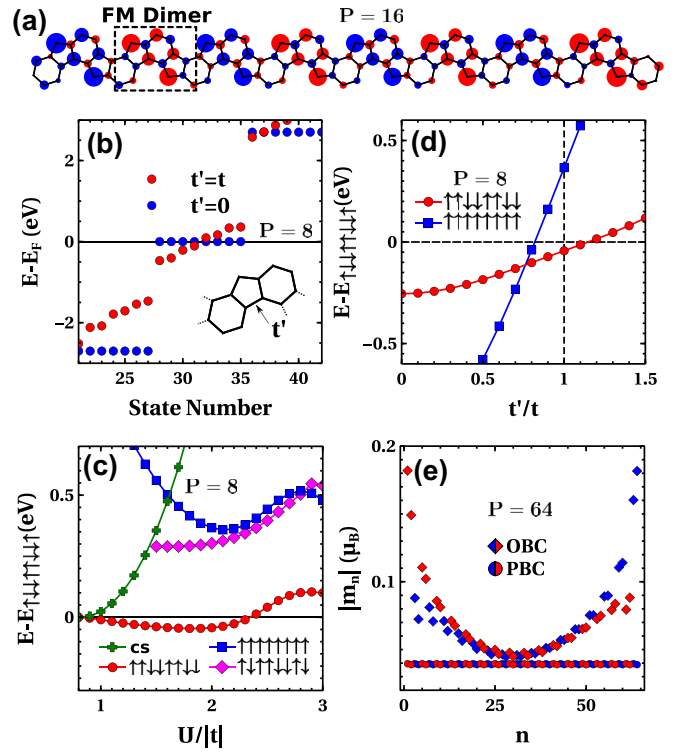


FIG. 2. (a) Magnetic moments m_i per carbon site i of the lowest-energy solution calculated for $U = 1.5|t|$ with the MF-Hubbard model, isomer 1 with $P = 16$ pentagons. Color stands for the sign and the area for the relative magnitude of the moment. (b) TB single-particle spectra ($U = 0$) for isomer 1 with $P = 8$. (c) Energy difference for different magnetic solutions and the broken dimers solution as a function of U , and (d) energy difference for the $\uparrow\uparrow\downarrow\uparrow\uparrow\downarrow$ (FM dimers) and $\uparrow\uparrow\uparrow\uparrow\uparrow\uparrow$ (FM) solutions and the broken dimers as a function of t' for $U = 2|t|$, converged with MF-Hubbard for isomer 1 with $P = 8$. (e) Absolute magnetic moments at each pentagon vertex n of the lowest-energy solution (FM dimers) for isomer 1 with $U = 0.85|t|$ and $P = 64$, considering both periodic (PBC) and open (OBC) boundary conditions. The red/blue colors stand for the sign of each moment.

MF-Hubbard model calculation for a $P = 8$ molecule when $U > 0.8|t|$ [Fig. 2(c)]. Counterintuitively, these pentagon moments do not display either ferromagnetism or antiferromagnetism, but instead they organize as FM dimers with AF order, distributed all over the chain [Fig. 2(a)]. The stability of these dimers can be tested by modulating t' , where they are the ground state in isomer 1 when $0.75 < t'/t < 1.15$, showing that a certain range of hybridization is key for their existence [Fig. 2(d)].

In Fig. 2(c) we show the energy difference between some magnetic solutions of an isomer 1 $P = 8$ molecule (labeled as $\sigma_1\sigma_2\dots\sigma_P$, where σ_n is the sign of the moment at the n th pentagon vertex) and a solution with, apparently, FM dimers throughout the molecule, except the edges ($\uparrow\downarrow\downarrow\uparrow\uparrow\downarrow\uparrow$, hereafter broken dimers), as a function of the on-site Coulomb repulsion U . After the system turns magnetic, the solution with the maximum number of FM dimers dominates with a maximum energy difference of 46 meV for $U \approx 1.8|t|$. This representation reveals the stabilization inherent to the

TABLE I. Energy differences ΔE for the different magnetic solutions of isomer **1** and the FM dimers, calculated with DFT (QE) and the PBE functional. As a reference, numbers in parenthesis are the corresponding results with the hybrid PBE0 functional using ORCA. The energies of the one-dimensional (periodic) polymer are referred to the unit cell, which included four pentagons. The relaxed geometry of the FM dimers solution was used for calculating all the magnetic phases, calculated for each length and functional. The broken dimers correspond to $\uparrow\downarrow\downarrow\uparrow$, $\uparrow\downarrow\uparrow\downarrow\uparrow\downarrow$, and $\uparrow\downarrow\uparrow\downarrow\uparrow\downarrow\uparrow\downarrow$ for $P = 4, 6$, and 8 , respectively.

	$P = 4$	$P = 6$	$P = 8$	1D
Broken dimers	2 (94)	39 (118)	18 (134)	–
Closed shell	2 (505)	119 (1153)	41 (1085)	29
FM ($S = P/2$)	654 (293)	855 (511)	1317 (741)	742

formation of the dimers, since a solution $\uparrow\downarrow\uparrow\downarrow\uparrow\downarrow\uparrow\downarrow$ with just two dimers is higher in energy and $\uparrow\downarrow\uparrow\downarrow\uparrow\downarrow\uparrow\downarrow$ could not be converged. If we keep increasing U , the dimer stability is compromised, so they are the ground state for $0.8|t| < U < 2.3|t|$, which includes the range that is usually taken to be physically relevant for nanographenes [49]. Additionally, we compute the FM phase with $S = P/2$, which is a higher energy solution until $U \approx 3.5|t|$ (not shown) that becomes the ground state.

We also performed DFT calculations for isomer **1** with different lengths and exchange-correlation functionals (see Table I). In all cases the FM dimers were the most stable solution (Fig. S1) [57]. Nonetheless, with the PBE functional, for the $P = 4$ molecule the difference with $\uparrow\downarrow\downarrow\uparrow$ is just 2.2 meV, and 2.1 meV with the closed-shell solution, which may shed doubts about a spin-polarized configuration as the lowest-energy state. However, for either larger polymers or with the PBE0 hybrid functional, this energy separation increased, which validates the FM dimers as the ground state, as we obtained with the MF-Hubbard model.

We want to point out one further remarkable feature of these polymers. In Fig. 2(e) we represent the absolute value of the magnetic moment at each pentagon vertex n for a large isomer **1** molecule with $P = 64$, calculated with the MF-Hubbard model for a low on-site Coulomb repulsion [58] ($U = 0.85|t|$). With periodic boundary conditions (PBC), positive and negative moments of equal magnitude alternate every two pentagons. When the edges are present, we can see that while they keep the same dimeric pattern, the magnetic moments get strongly localized at the termini, suggesting nontrivial topology.

In order to understand the physics behind this magnetic behavior, it is useful to consider these systems as just bipartite lattices composed of hexagons, linked by an extra carbon atom, plus an additional hopping that completes the ladder backbone [48]. Then, for $P = 1$ and $t' = 0$, we have a nanographene that consists of two hexagons with one carbon that serves as linker. Such a molecule displays sublattice imbalance and one zero mode mainly localized at the carbon atom that links the hexagons [Fig. 3(a)]. All the isomers are formed depending on the position and the rotation of the bond that connects to the next linker. For instance, the molecule at

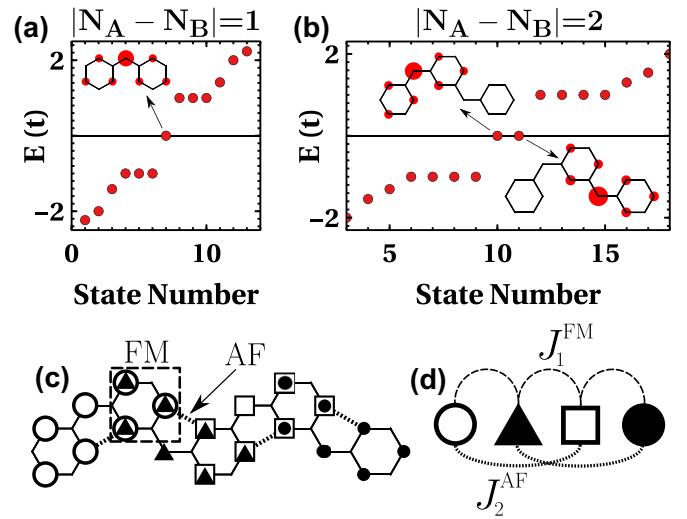


FIG. 3. [(a), (b)] TB spectra ($U = 0$) of two OInIn with $P = 1$ and $P = 2$, both with $t' = 0$. The insets stand for the probability distribution of the zero modes. (c) Sketch of these zero modes on a lattice of isomer **1**. (d) Effective spin-1/2 model that isomer **1** can be mapped to, according to this analysis.

the inset of Fig. 3(b) corresponds to isomer **1** with $P = 2$ and $t' = 0$. In this case, the second linker adds an extra atom to the majority sublattice, and therefore $|N_A - N_B| = 2$. Interestingly, the wave functions of the degenerate zero modes can be chosen to be localized in a similar way as that of the previous $P = 1$ molecule.

As a consequence, an isomer **1** polymer with P pentagons and $t' = 0$ has P zero modes, each one of them localized at one linker and, to a lesser degree, at the adjacent hexagons. This is schematically represented in Fig. 3(c), from which we can infer three main magnetic interactions when t' is included in the picture. First, two first-neighboring unpaired electrons share one hexagon, where their wave functions overlap, leading to a FM Hund's interaction [30] that scales with U . Second, t' hopping promotes a kinetic Anderson AF exchange [30], proportional to $1/U$, that happens between first- and second-neighbors. Summarizing: isomer **1** presents competing AF and FM first-neighbor interactions and AF second-neighbor interaction between the unpaired electrons.

The fact that we converge FM dimers as the lowest-energy phase of isomer **1** is not trivial, since dimerization may happen as a result of magnetic frustration. Actually, two examples where dimerization occurs in the ground state are the frustrated $S = 1/2$ Heisenberg chains with second-neighbor AF exchange and either AF or FM first-neighbor interactions [59–65]:

$$\mathcal{H} = J_1 \sum_{\langle i,j \rangle} \vec{S}_i \cdot \vec{S}_j + J_2^{\text{AF}} \sum_{\langle\langle i,j \rangle\rangle} \vec{S}_i \cdot \vec{S}_j, \quad (1)$$

where \vec{S}_i is the spin operator vector and $\langle i, j \rangle$ ($\langle\langle i, j \rangle\rangle$) runs over first (second) neighboring spins with J_1 (J_2^{AF}) magnetic exchange.

Hence, Eq. (1) contains two scenarios. First, when $J_1 \equiv J_1^{\text{AF}} > 0$, the model can be exactly solved at the

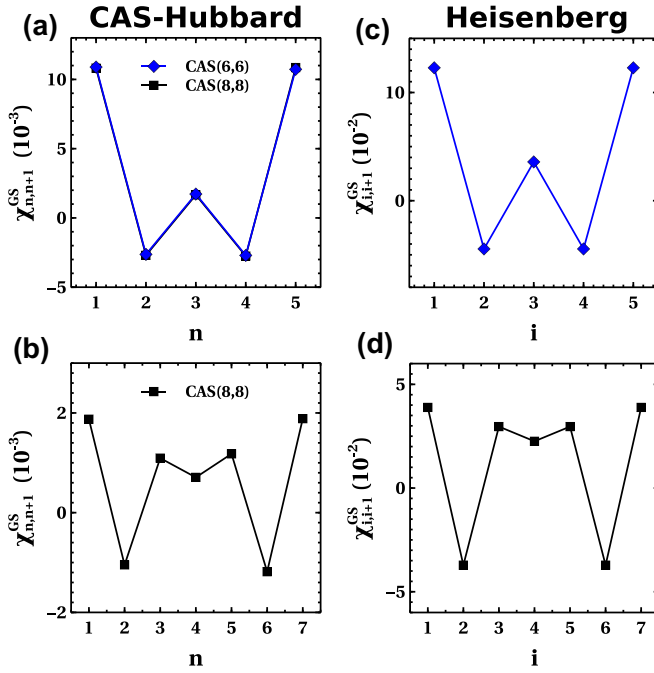


FIG. 4. [(a), (b)] Spin correlators between the vertex atom of first-neighboring pentagons for isomer **1** molecules with different sizes and $U = 1.5|t|$. (c, d) Spin correlators between first-neighboring $S = 1/2$ spins of the frustrated FM chain with second-neighbor AF exchange and $J_1^{\text{FM}} = -2J_2^{\text{AF}}$.

Majumdar-Ghosh point [59–63] ($J_1^{\text{AF}} = 2J_2^{\text{AF}}$), and the ground state consists of a valence-bond solid (VBS) of singlets that served as inspiration of the Affleck-Kennedy-Lieb-Tasaki (AKLT) model [66]. Second, considering PBC, in the $J_1 \equiv J_1^{\text{FM}} < 0$ case [64,65] one finds two regimes: $|J_1^{\text{FM}}/J_2^{\text{AF}}| > 4$, where the ground state is the FM solution, and $|J_1^{\text{FM}}/J_2^{\text{AF}}| < 4$, where frustration promotes a process of order by disorder [67] that leads to a VBS of FM dimers [64] with spin singlets between third neighbors [65]. Interestingly, since these FM dimers effectively behave as $S = 1$ spins, this phase has a hidden topological order similar to the AKLT model, showing a spin gap and edge-spin fractionalization [65].

Therefore, considering that when U increases the FM eventually surpasses the AF first-neighbor interaction, isomer **1** can be described by a frustrated FM $S = 1/2$ Heisenberg chain. This scenario, illustrated in Fig. 3(d), along with the results shown in Fig. 2, leads us to suggest that the FM dimers shown so far are, indeed, such VBS, and the edge magnetization originates in the fractionalization of an effective Haldane chain [66].

In order to confirm this statement, we calculate spin correlators with a CAS-Hubbard model between the different unpaired electrons in isomer **1** and compare them with those between neighboring spins in the frustrated FM Heisenberg chain (Figs. 4 and S4) [57]. To do this, we first compute the multifigural eigenstates from an exact Hubbard model of isomer **1** with $U = 1.5|t|$. Since the VBS from polymers with $P = 4m$, where m is an integer, must be a singlet, we cannot use $\langle S_z(i) \rangle$ to assess the magnetic moment. Instead,

we compute the spin correlator:

$$\chi_{i,j}^{\Psi} = \langle \Psi | S_z(i) S_z(j) | \Psi \rangle, \quad (2)$$

where $S_z(i)$ is the z -component of the spin operator at site i and Ψ is a many-body wave function, between each pair of pentagon-vertices $i = n$ and $j = n + 1$ that are separated by one hexagon.

In Figs. 4(a) and 4(b) we show the correlators between the adjacent unpaired electrons in isomer **1**. Ψ is chosen to be the ground state, which changes spin multiplicity (Fig. S5) [57] depending on U . Since we are looking for the FM-dimers phase, the selected U was inside a range where the polymers with $P = 4m$ ($P = 4m + 2$) have an $S = 0$ ($S = 1$) ground state that depends on whether the VBS has even or odd number of dimers. In the left panels of Fig. 4 we can clearly see the formation of the FM dimers, in qualitative agreement with the correlators between neighboring spins of the frustrated FM Heisenberg chain [Figs. 4(c) and 4(d)].

We want to stress the possibility of doing a similar analysis as that of Fig. 3 for the other isomers (Fig. S7) [57]. In this sense we may anticipate their magnetic properties by means of their sublattice imbalance when $t' = 0$, which leads to the classification in Fig. 1. Isomers **2** and **3** have sublattice imbalance, their unpaired electrons overlap, and they belong to the same class as isomer **1**. On the other hand, in isomers **4**, **5**, and **6**, with $|N_A - N_B| = 0$, unpaired electrons are connected by first-neighbor hopping. Here, the closure of the pentagon does not add any significant interaction, and hence these isomers cannot be described by a frustrated chain but by a TB chain instead (Figs. S8, S9, and S10) [57]. Thus the energy separation between the highest occupied and lowest unoccupied molecular orbitals decreases with the length, which stabilizes the AF spin-polarized solution as the ground state (Fig. S2) [57], in agreement with the notion that $P = 2$ molecules of class **II** are closed shell [38,68] and become magnetic when the size of the polymer is increased [36,40,41].

Class **I** isomers, on the other hand, are more complicated. In the literature [69] the smallest island of isomer **1** is expected to be a triplet, which agrees with our results, but isomer **2** with $P = 2$ is predicted to be an open-shell singlet [68,70]. This can be explained if we consider that the larger hybridization in isomer **2** [Fig. S3(a)] [57] strengthens the AF first-neighbor interactions enough to not be surpassed by the FM exchange. If that is the situation, the system can be described with an $S = 1/2$ AF Heisenberg chain with AF second-neighbor exchange, which justifies the $S = 0$ solution of the $P = 2$ island, and anticipates different physics for isomer **2**, despite it belonging to the same class as isomer **1**.

This model, for larger chains and away from the Majumdar-Ghosh point, exhibits two distinct phases. When $J_1^{\text{AF}} > 2J_2^{\text{AF}}$, the numerical ground state consists in singlet dimers with a weak AF correlation, which is clearly seen in calculations of spin correlators calculated with the CAS-Hubbard model (Fig. S6) [57]. On the other hand, when $J_1^{\text{AF}} < 2J_2^{\text{AF}}$, the singlet dimers are ferromagnetically correlated [71], which looks like the broken dimers $\uparrow\downarrow\uparrow\downarrow\uparrow\downarrow\uparrow\downarrow$ ground state from the MF-Hubbard of isomer **2** with $P = 8$ at $1.53|t| < U < 2.57|t|$ [Fig. S3(c)] [57]. However, the effective $\tilde{U}/|\tilde{t}|$ ratio [35] for isomer **1** (**2**) is 16.5 (1.8) for $U = 1.5|t|$ (where $\tilde{t} = \langle z_1 | \mathcal{H}_t | z_2 \rangle$, $\tilde{U} = U \sum_i |z_{1,2}(i)|^4$, and $z_{1,2}$ are two adjacent

zero modes of molecules with $t' = 0$). Since the open-shell picture gets obscured [30] if \tilde{U} is not at least a few times larger than $|\tilde{t}|$, the description by a spin chain for isomer **2** may be compromised, concluding that further theoretical effort is needed to actually assess its ground state.

Finally, we explore a little further the idea that the FM dimers are unstable due to electron hybridization. As shown in the Supplemental Material [Fig. S3(e)] [57], by decreasing t' it is possible to obtain the FM dimers as the ground state in isomer **2**, but this modulation of t' seems unrealistic for a real carbon bond. Instead, by adding an additional hexagon between each pair of pentagons [Figs. S3(b), S3(d), and S3(f)] [57], the lower single-particle gap opens for $t' = t$ and the FM dimers are now the ground state for a broader window of U and in the $t' \approx t$ vicinity. These results show that by decreasing the hybridization, the description by the frustrated FM chain becomes more feasible. Then the FM dimers become stabilized, but also the FM phase, which is the ground state for $U > 2.0|t|$.

Conclusions. We have presented the FM dimers as the ground state of isomer **1**, with characteristic magnetic localization at the termini that suggests fractionalization. To understand this behavior, we performed an analysis of the magnetic interactions that classifies the isomers into either class **I** with competing FM and AF first-neighbor exchange and second-neighbor AF exchange, or class **II** with first-neighbor AF exchange only.

The sign and range of these magnetic interactions are enough to explain the results obtained for isomers **1** and **3**, since the lowest-energy solution (FM dimers) can be identified as the VBS ground state of the $S = 1/2$ FM Heisenberg chain with AF second-neighbor exchange. The antiferromagnetic ground state of isomers **4**, **5**, and **6** is also justified by the magnetic interactions shown here. Recently, a spin-polarized tip has been used to probe the spin polarization in chiral graphene nanoribbons [72], which may also reveal the ground state of isomers **1** and **3** in a feasible experiment. This way it should be possible to determine the spin alignment of the FM dimers phase, and not just through the presence of fractionalization at the termini of the chains.

Our results provide a general framework for understanding magnetism in (non-benzenoid) planar carbon nanostructures with pentagons, paving the way for the realization of further exotic spin physics such as, for instance, two-dimensional networks with spin frustration that might be spin liquid candidates.

Acknowledgments. We thank Pavel Jelínek for fruitful discussions. This work was funded by the Spanish MCIN/AEI/10.13039/501100011033 (PID2020-115406GB-I00), the Basque Department of Education (IKUR Strategy under the collaboration agreement between Ikerbasque and DIPC), and the European Union's Horizon 2020 Program (FET-Open project SPRING Grant No. 863098).

-
- [1] Y. Cao, V. Fatemi, S. Fang, K. Watanabe, T. Taniguchi, E. Kaxiras, and P. Jarillo-Herrero, Unconventional superconductivity in magic-angle graphene superlattices, *Nature (London)* **556**, 43 (2018).
- [2] S. Mishra, G. Catarina, F. Wu, R. Ortiz, D. Jacob, K. Eimre, J. Ma, C. A. Pignedoli, X. Feng, P. Ruffieux *et al.*, Observation of fractional edge excitations in nanographene spin chains, *Nature (London)* **598**, 287 (2021).
- [3] S. Mishra, D. Beyer, K. Eimre, R. Ortiz, J. Fernández-Rossier, R. Berger, O. Gröning, C. A. Pignedoli, R. Fasel, X. Feng *et al.*, Collective all-carbon magnetism in triangulene dimers, *Angew. Chem. Int. Ed.* **59**, 12041 (2020).
- [4] D. J. Rizzo, G. Veber, J. Jiang, R. McCurdy, T. Cao, C. Bronner, T. Chen, S. G. Louie, F. R. Fischer, and M. F. Crommie, Inducing metallicity in graphene nanoribbons via zero-mode superlattices, *Science* **369**, 1597 (2020).
- [5] Q. Sun, O. Gröning, J. Overbeck, O. Braun, M. L. Perrin, G. Borin Barin, M. El Abbassi, K. Eimre, E. Ditler, C. Daniels, V. Meunier, C. A. Pignedoli, M. Calame, R. Fasel, and P. Ruffieux, Massive Dirac fermion behavior in a low bandgap graphene nanoribbon near a topological phase boundary, *Adv. Mater.* **32**, 1906054 (2020).
- [6] Q. Sun, X. Yao, O. Gröning, K. Eimre, C. A. Pignedoli, K. Müllen, A. Narita, R. Fasel, and P. Ruffieux, Coupled spin states in armchair graphene nanoribbons with asymmetric zigzag edge extensions, *Nano Lett.* **20**, 6429 (2020).
- [7] Q. Sun, Y. Yan, X. Yao, K. Müllen, A. Narita, R. Fasel, and P. Ruffieux, Evolution of the topological energy band in graphene nanoribbons, *J. Phys. Chem. Lett.* **12**, 8679 (2021).
- [8] J. Hieuille, S. Castro, N. Friedrich, A. Vegliante, F. R. Lara, S. Sanz, D. Rey, M. Corso, T. Frederiksen, J. I. Pascual, and D. Peña, On-surface synthesis and collective spin excitations of a triangulene-based nanostar, *Angew. Chem. Int. Ed.* **60**, 25224 (2021).
- [9] O. Gröning, S. Wang, X. Yao, C. A. Pignedoli, G. Borin Barin, C. Daniels, A. Cupo, V. Meunier, X. Feng, A. Narita *et al.*, Engineering of robust topological quantum phases in graphene nanoribbons, *Nature (London)* **560**, 209 (2018).
- [10] R. Ortiz, J. C. Sancho-García, and J. Fernández-Rossier, Frustrated magnetic interactions in a cyclacene crystal, *Phys. Rev. Mater.* **6**, 014406 (2022).
- [11] G. Catarina and J. Fernández-Rossier, Hubbard model for spin-1 Haldane chains, *Phys. Rev. B* **105**, L081116 (2022).
- [12] R. Ortiz, G. Catarina, and J. Fernández-Rossier, Theory of triangulene two-dimensional crystals, *2D Mater.* **10**, 015015 (2023).
- [13] S. Wang, L. Talirz, C. A. Pignedoli, X. Feng, K. Müllen, R. Fasel, and P. Ruffieux, Giant edge state splitting at atomically precise graphene zigzag edges, *Nat. Commun.* **7**, 11507 (2016).
- [14] P. Ruffieux, S. Wang, B. Yang, C. Sánchez-Sánchez, J. Liu, T. Dienel, L. Talirz, P. Shinde, C. A. Pignedoli, D. Passerone, T. Dumlaff, X. Feng, K. Müllen, and R. Fasel, On-surface synthesis of graphene nanoribbons with zigzag edge topology, *Nature (London)* **531**, 489 (2016).
- [15] N. Pavliček, A. Mistry, Z. Majzik, N. Moll, G. Meyer, D. J. Fox, and L. Gross, Synthesis and characterization of triangulene, *Nat. Nanotechnol.* **12**, 308 (2017).
- [16] S. Mishra, T. G. Lohr, C. A. Pignedoli, J. Liu, R. Berger, J. I. Urgel, K. Müllen, X. Feng, P. Ruffieux, and R. Fasel, Tailoring

- bond topologies in open-shell graphene nanostructures, *ACS Nano* **12**, 11917 (2018).
- [17] J. Li, S. Sanz, M. Corso, D. J. Choi, D. Peña, T. Frederiksen, and J. I. Pascual, Single spin localization and manipulation in graphene open-shell nanostructures, *Nat. Commun.* **10**, 200 (2019).
- [18] J. Li, S. Sanz, J. Castro-Esteban, M. Vilas-Varela, N. Friedrich, T. Frederiksen, D. Peña, and J. I. Pascual, Uncovering the Triplet Ground State of Triangular Graphene Nanoflakes Engineered with Atomic Precision on a Metal Surface, *Phys. Rev. Lett.* **124**, 177201 (2020).
- [19] S. Mishra, D. Beyer, R. Berger, J. Liu, O. Gröning, J. I. Urgel, K. Müllen, P. Ruffieux, X. Feng, and R. Fasel, Topological defect-induced magnetism in a nanographene, *J. Am. Chem. Soc.* **142**, 1147 (2020).
- [20] S. Mishra, X. Yao, Q. Chen, K. Eimre, O. Gröning, R. Ortiz, M. Di-Giovannantonio, S.-G. J. Carlos, J. Fernández-Rossier, C. A. Pignedoli, K. Müllen, P. Ruffieux, A. Narita, and R. Fasel, Large magnetic exchange coupling in rhombus-shaped nanographenes with zigzag periphery, *Nat. Chem.* **13**, 581 (2021).
- [21] S. Mishra, D. Beyer, K. Eimre, S. Kezilebieke, R. Berger, O. Gröning, C. A. Pignedoli, K. Müllen, P. Liljeroth, P. Ruffieux *et al.*, Topological frustration induces unconventional magnetism in a nanographene, *Nat. Nanotechnol.* **15**, 22 (2020).
- [22] R. Ortiz and J. Fernández-Rossier, Probing local moments in nanographenes with electron tunneling spectroscopy, *Prog. Surf. Sci.* **95**, 100595 (2020).
- [23] S. Song, J. Su, M. Telychko, J. Li, G. Li, Y. Li, C. Su, J. Wu, and J. Lu, On-surface synthesis of graphene nanostructures with π -magnetism, *Chem. Soc. Rev.* **50**, 3238 (2021).
- [24] D. G. de Oteyza and T. Frederiksen, Carbon-based nanostructures as a versatile platform for tunable π -magnetism, *J. Phys.: Condens. Matter* **34**, 443001 (2022).
- [25] J. Lado, N. García-Martínez, and J. Fernández-Rossier, Edge states in graphene-like systems, *Synth. Met.* **210**, 56 (2015), Reviews of Current Advances in Graphene Science and Technology.
- [26] J. Fernández-Rossier and J. J. Palacios, Magnetism in Graphene Nanoislands, *Phys. Rev. Lett.* **99**, 177204 (2007).
- [27] M. Koshino, T. Morimoto, and M. Sato, Topological zero modes and Dirac points protected by spatial symmetry and chiral symmetry, *Phys. Rev. B* **90**, 115207 (2014).
- [28] T. Cao, F. Zhao, and S. G. Louie, Topological Phases in Graphene Nanoribbons: Junction States, Spin Centers, and Quantum Spin Chains, *Phys. Rev. Lett.* **119**, 076401 (2017).
- [29] R. Ortiz, R. Á. Boto, N. García-Martínez, J. C. Sancho-García, M. Melle-Franco, and J. Fernández-Rossier, Exchange rules for diradical π -conjugated hydrocarbons, *Nano Lett.* **19**, 5991 (2019).
- [30] D. Jacob and J. Fernández-Rossier, Theory of intermolecular exchange in coupled spin- $\frac{1}{2}$ nanographenes, *Phys. Rev. B* **106**, 205405 (2022).
- [31] E. H. Lieb, Two Theorems on the Hubbard Model, *Phys. Rev. Lett.* **62**, 1201 (1989).
- [32] L. Cusinato, S. Evangelisti, T. Leininger, and A. Monari, The electronic structure of graphene nanoislands: A CAS-SCF and NEVPT2 study, *Adv. Condens. Matter Phys.* (2018) 9097045.
- [33] R. Ortiz, J. L. Lado, M. Melle-Franco, and J. Fernández-Rossier, Engineering spin exchange in nonbipartite graphene zigzag edges, *Phys. Rev. B* **94**, 094414 (2016).
- [34] P. W. Anderson, New approach to the theory of superexchange interactions, *Phys. Rev.* **115**, 2 (1959).
- [35] R. Ortiz, N. A. García-Martínez, J. L. Lado, and J. Fernández-Rossier, Electrical spin manipulation in graphene nanostructures, *Phys. Rev. B* **97**, 195425 (2018).
- [36] Z. Majzik, N. Pavliček, M. Vilas-Varela, D. Pérez, N. Moll, E. Guitián, G. Meyer, D. Peña, and L. Gross, Studying an antiaromatic polycyclic hydrocarbon adsorbed on different surfaces, *Nat. Commun.* **9**, 1198 (2018).
- [37] M. Di Giovannantonio, Q. Chen, J. I. Urgel, P. Ruffieux, C. A. Pignedoli, K. Müllen, A. Narita, and R. Fasel, On-surface synthesis of oligo(indenoidene), *J. Am. Chem. Soc.* **142**, 12925 (2020).
- [38] K. Fukuda, T. Nagami, J.-Y. Fujiyoshi, and M. Nakano, Interplay between open-shell character, aromaticity, and second hyperpolarizabilities in indenofluorenes, *J. Phys. Chem. A* **119**, 10620 (2015).
- [39] S. Thomas and K. S. Kim, Linear and nonlinear optical properties of indeno[2,1-*b*]fluorene and its structural isomers, *Phys. Chem. Chem. Phys.* **16**, 24592 (2014).
- [40] M. Yamane, R. Kishi, T. Tonami, K. Okada, T. Nagami, Y. Kitagawa, and M. Nakano, Open-shell characters, aromaticities and third-order nonlinear optical properties of carbon nanobelts composed of five- and six-membered rings, *Asian J. Org. Chem.* **7**, 2320 (2018).
- [41] K. Fukuda, J.-Y. Fujiyoshi, H. Matsui, T. Nagami, S. Takamuku, Y. Kitagawa, B. Champagne, and M. Nakano, A theoretical study on quasi-one-dimensional open-shell singlet ladder oligomers: Multi-radical nature, aromaticity and second hyperpolarizability, *Org. Chem. Front.* **4**, 779 (2017).
- [42] S. Mishra, S. Fatayer, S. Fernández, K. Kaiser, D. Peña, and L. Gross, Nonbenzenoid high-spin polycyclic hydrocarbons generated by atom manipulation, *ACS Nano* **16**, 3264 (2022).
- [43] C. Li, Y. Liu, Y. Liu, F.-H. Xue, D. Guan, Y. Li, H. Zheng, C. Liu, J. Jia, P.-N. Liu *et al.*, Topological defects induced high-spin quartet state in truxene-based molecular graphenoids, *CCS Chem.* **5**, 695 (2023).
- [44] M. Di Giovannantonio, K. Eimre, A. V. Yakutovich, Q. Chen, S. Mishra, J. I. Urgel, C. A. Pignedoli, P. Ruffieux, K. Müllen, A. Narita, and R. Fasel, On-surface synthesis of antiaromatic and open-shell indeno[2,1-*b*]fluorene polymers and their lateral fusion into porous ribbons, *J. Am. Chem. Soc.* **141**, 12346 (2019).
- [45] M. Di Giovannantonio, J. I. Urgel, U. Beser, A. V. Yakutovich, J. Wilhelm, C. A. Pignedoli, P. Ruffieux, A. Narita, K. Müllen, and R. Fasel, On-surface synthesis of indenofluorene polymers by oxidative five-membered ring formation, *J. Am. Chem. Soc.* **140**, 3532 (2018).
- [46] P. Hu, S. Lee, T. S. Heng, N. Aratani, T. P. Gonçalves, Q. Qi, X. Shi, H. Yamada, K.-W. Huang, J. Ding *et al.*, Toward tetraradicaloid: The effect of fusion mode on radical character and chemical reactivity, *J. Am. Chem. Soc.* **138**, 1065 (2016).
- [47] C.-N. Yeh and J.-D. Chai, Role of Kekulé and non-Kekulé structures in the radical character of alternant polycyclic aromatic hydrocarbons: A TAO-DFT study, *Sci. Rep.* **6**, 1 (2016).
- [48] M. Kertesz, Structure and electronic structure of low-band-gap ladder polymers, *Macromolecules* **28**, 1475 (1995).
- [49] O. V. Yazzev, Emergence of magnetism in graphene materials and nanostructures, *Rep. Prog. Phys.* **73**, 056501 (2010).

- [50] P. Giannozzi, S. Baroni, N. Bonini, M. Calandra, R. Car, C. Cavazzoni, D. Ceresoli, G. L. Chiarotti, M. Cococcioni, I. Dabo *et al.*, Quantum ESPRESSO: A modular and open-source software project for quantum simulations of materials, *J. Phys.: Condens. Matter* **21**, 395502 (2009).
- [51] P. Giannozzi, O. Andreussi, T. Brumme, O. Bunau, M. B. Nardelli, M. Calandra, R. Car, C. Cavazzoni, D. Ceresoli, M. Cococcioni *et al.*, Advanced capabilities for materials modelling with Quantum ESPRESSO, *J. Phys.: Condens. Matter* **29**, 465901 (2017).
- [52] P. Giannozzi, O. Baseggio, P. Bonfà, D. Brunato, R. Car, I. Carnimeo, C. Cavazzoni, S. de Gironcoli, P. Delugas, F. Ferrari Ruffino, A. Ferretti, N. Marzari, I. Timrov, A. Urru, and S. Baroni, Quantum ESPRESSO toward the exascale, *J. Chem. Phys.* **152**, 154105 (2020).
- [53] J. P. Perdew, K. Burke, and M. Ernzerhof, Generalized Gradient Approximation Made Simple, *Phys. Rev. Lett.* **77**, 3865 (1996).
- [54] F. Neese, The ORCA program system, *WIREs Comput. Mol. Sci.* **2**, 73 (2012).
- [55] J. P. Perdew, M. Ernzerhof, and K. Burke, Rationale for mixing exact exchange with density functional approximations, *J. Chem. Phys.* **105**, 9982 (1996).
- [56] C. Adamo and V. Barone, Toward reliable density functional methods without adjustable parameters: The PBE0 model, *J. Chem. Phys.* **110**, 6158 (1999).
- [57] See Supplemental Material <http://link.aps.org/supplemental/10.1103/PhysRevB.107.L100416> for details, which includes Refs. [73–84].
- [58] We choose $U = 0.85|t| < |t|$ to show the presence of edge magnetization, since for higher values of U these edge-localized moments are obscured by the magnetism originated by low-energy electrons in the other pentagons.
- [59] C. K. Majumdar and D. K. Ghosh, On next-nearest-neighbor interaction in linear chain. I, *J. Math. Phys.* **10**, 1388 (1969).
- [60] C. K. Majumdar, Antiferromagnetic model with known ground state, *J. Phys. C: Solid State Phys.* **3**, 911 (1970).
- [61] F. D. M. Haldane, Spontaneous dimerization in the $S = 1/2$ Heisenberg antiferromagnetic chain with competing interactions, *Phys. Rev. B* **25**, 4925 (1982).
- [62] P. M. van den Broek, Exact value of the ground state energy of the linear antiferromagnetic Heisenberg chain with nearest and next-nearest neighbour interactions, *Phys. Lett. A* **77**, 261 (1980).
- [63] H.-Z. Xu, S.-Y. Zhang, G.-C. Guo, and M. Gong, Exact dimer phase with anisotropic interaction for one dimensional magnets, *Sci. Rep.* **11**, 6462 (2021).
- [64] S. Furukawa, M. Sato, S. Onoda, and A. Furusaki, Ground-state phase diagram of a $S = 1/2$ frustrated ferromagnetic XXZ chain: Haldane dimer phase and gapped/gapless chiral phases, *Phys. Rev. B* **86**, 094417 (2012).
- [65] C. E. Agrapidis, S.-L. Drechsler, J. van den Brink, and S. Nishimoto, Coexistence of valence-bond formation and topological order in the frustrated ferromagnetic j_1 - j_2 chain, *SciPost Phys.* **6**, 019 (2019).
- [66] I. Affleck, T. Kennedy, E. H. Lieb, and H. Tasaki, Valence bond ground states in isotropic quantum antiferromagnets, *Commun. Math. Phys.* **115**, 477 (1988).
- [67] J. Villain, R. Bidaux, J.-P. Carton, and R. Conte, Order as an effect of disorder, *J. Phys. France* **41**, 1263 (1980).
- [68] A. Shimizu, S. Nobusue, H. Miyoshi, and Y. Tobe, Indenofluorene cogeners: Biradicaloids and beyond, *Pure Appl. Chem.* **86**, 517 (2014).
- [69] J. J. Dressler, Z. Zhou, J. L. Marshall, R. Kishi, S. Takamuku, Z. Wei, S. N. Spisak, M. Nakano, M. A. Petrukhina, and M. M. Haley, Synthesis of the unknown indenol[1, 2-*a*]fluorene regioisomer: Crystallographic characterization of its dianion, *Angew. Chem.* **129**, 15565 (2017).
- [70] A. Shimizu, R. Kishi, M. Nakano, D. Shiomi, K. Sato, T. Takui, I. Hisaki, M. Miyata, and Y. Tobe, Indeno[2,1-*b*]fluorene: A 20- π -electron hydrocarbon with very low-energy light absorption, *Angew. Chem.* **125**, 6192 (2013).
- [71] S. R. White and I. Affleck, Dimerization and incommensurate spiral spin correlations in the zigzag spin chain: Analogies to the Kondo lattice, *Phys. Rev. B* **54**, 9862 (1996).
- [72] J. Brede, N. Merino-Díez, A. Berdonces, S. Sanz, A. Domínguez-Celorrío, J. Lobo-Checa, M. Vilas-Varela, D. Peña, T. Frederiksen, J. I. Pascual, D. G. de Oteyza, and D. Serrate, Detecting the spin-polarization of edge states in graphene nanoribbons, [arXiv:2301.11370](https://arxiv.org/abs/2301.11370).
- [73] J. Fernández-Rossier, Prediction of hidden multiferroic order in graphene zigzag ribbons, *Phys. Rev. B* **77**, 075430 (2008).
- [74] M. Fujita, K. Wakabayashi, K. Nakada, and K. Kusakabe, Peculiar localized state at zigzag graphite edge, *J. Phys. Soc. Jpn.* **65**, 1920 (1996).
- [75] K. Wakabayashi, M. Sigrist, and M. Fujita, Spin wave mode of edge-localized magnetic states in nanographite zigzag ribbons, *J. Phys. Soc. Jpn.* **67**, 2089 (1998).
- [76] F. Muñoz-Rojas, J. Fernández-Rossier, and J. J. Palacios, Giant Magnetoresistance in Ultrasmall Graphene Based Devices, *Phys. Rev. Lett.* **102**, 136810 (2009).
- [77] O. V. Yazyev, R. B. Capaz, and S. G. Louie, Theory of magnetic edge states in chiral graphene nanoribbons, *Phys. Rev. B* **84**, 115406 (2011).
- [78] D. Soriano and J. Fernández-Rossier, Spontaneous persistent currents in a quantum spin Hall insulator, *Phys. Rev. B* **82**, 161302(R) (2010).
- [79] Y. Shen and C.-F. Chen, Helicenes: Synthesis and applications, *Chem. Rev.* **112**, 1463 (2012).
- [80] B. C. Baciú, T. de Ara, C. Sabater, C. Untiedt, and A. Guíjarro, Helical nanostructures for organic electronics: The role of topological sulfur in *ad hoc* synthesized dithia[7]helicenes studied in the solid state and on a gold surface, *Nanoscale Adv.* **2**, 1921 (2020).
- [81] N. Marzari, D. Vanderbilt, A. De Vita, and M. C. Payne, Thermal Contraction and Disordering of the Al(110) Surface, *Phys. Rev. Lett.* **82**, 3296 (1999).
- [82] F. Neese, Definition of corresponding orbitals and the diradical character in broken symmetry DFT calculations on spin coupled systems, *J. Phys. Chem. Solids* **65**, 781 (2004).
- [83] F. Weigend and R. Ahlrichs, Balanced basis sets of split valence, triple zeta valence and quadruple zeta valence quality for H to Rn: Design and assessment of accuracy, *Phys. Chem. Chem. Phys.* **7**, 3297 (2005).
- [84] G. L. Stoychev, A. A. Auer, and F. Neese, Automatic generation of auxiliary basis sets, *J. Chem. Theory Comput.* **13**, 554 (2017).

Magnetic frustration and fractionalization in oligo(indenoindenes). Supplementary material.

Ricardo Ortiz,¹ Geza Giedke,^{1,2} and Thomas Frederiksen^{1,2}

¹*Donostia International Physics Center (DIPC), E-20018 San Sebastián, Spain*

²*IKERBASQUE, Basque Foundation for Science, E-48013, Bilbao, Spain*

(Dated: March 14, 2023)

CONTENTS

I. Methods	1
A. Hubbard model	1
B. Density functional theory	2
II. Mean-field Hubbard calculations for isomers 2, 3, 4, 5 and 6	4
III. CAS-Hubbard calculations	7
IV. Magnetic interactions analysis	9
References	11

I. METHODS

A. Hubbard model

The results reported in this article are obtained with several levels of theory. First, the electronic interactions are considered with the Hubbard model:

$$\mathcal{H} = \mathcal{H}_t + \mathcal{H}_U = t \sum_{\sigma \langle i,j \rangle} c_{i\sigma}^\dagger c_{j\sigma} + U \sum_i n_{i\uparrow} n_{i\downarrow}, \quad (1)$$

where the first part is the nearest-neighbours tight-binding Hamiltonian with hopping t , whilst the second counts electrons at each atomic orbital i and estimates the resulting on-site Coulomb repulsion with the parameter U .

We solve this model employing two different approaches. First, an exact diagonalization with a complete active space of molecular orbitals (CAS(N_e, N_o)), where N_e electrons fluctuate in N_o orbitals to form the configurations of the multielectronic basis. The CAS-Hubbard method has shown efficient to study excitation energies of radical nanographenes[1–3], where usually it is enough to include the non-bonding states in the active space to converge the low energy manifold (plus one valence and conduction state in some particular cases) [4].

Second, we employ a mean-field approximation of the Hubbard model, that replaces the electron-electron repulsion by an interaction with an effective potential. This approximation is well-known for offering similar results than DFT for nanographenes[5, 6], so it is also justified to study the ground state of OInIn. The exact Hamiltonian of the mean-field Hubbard model presents Hartree and Fock contributions[7], but an approximation where the latter is ignored, and just collinear solutions are considered, is often done[5, 8–13]. In consequence, we write the Hamiltonian as follows:

$$\mathcal{H} = \mathcal{H}_t + \mathcal{H}_{MF}, \quad (2)$$

$$\mathcal{H}_{MF} = U \sum_i (n_{i\uparrow} \langle n_{i\downarrow} \rangle + n_{i\downarrow} \langle n_{i\uparrow} \rangle), \quad (3)$$

where $\langle n_{i\sigma} \rangle$ is the electron density at orbital i , σ labels the spin and the magnetic moments are just the spin density:

$$m_i = \frac{\langle n_{i\uparrow} \rangle - \langle n_{i\downarrow} \rangle}{2}. \quad (4)$$

We also assume that all the systems studied in this work are planar, and therefore the orthogonal symmetry between decoupled σ and π orbitals allows us to consider just one p_z orbital per carbon atom. However, we warn the reader that whilst this assumption is a fair approximation for the straight polymers, originating from isomers **1** and **4**, it might not be for those from isomers **2**, **3**, **5** and **6**. As we can see in the first figure from the main text, the last mentioned are curved, and therefore large enough molecules will be forced to have a spiral geometry, similar to the helicene molecules[14, 15]. Here, we restrict ourselves to molecules without a 3D configuration, and the study of non-planar polymers will thus be out of the scope.

B. Density functional theory

We also compare the mean-field Hubbard results with those from Density Functional Theory (DFT) for the case of isomer **1**, employing Perdew-Burke-Ernzerhof[16] (PBE) exchange-correlation functional with Vanderbilt ultrasoft non-relativistic pseudopotential for carbon and hydrogen. These calculations are done with the Quantum ESPRESSO (QE) package[17–19], where all valence electrons are taken into account, along with long-range Coulomb interactions, the inclusion of H atoms, and the possibility of different bond lengths upon relaxation. The relaxed atomic positions, computed with the BFGS quasi-Newton algorithm and with a convergence pressure of 0.5 Kbar, did not deviate significantly from planarity, justifying the use of the previous methods. The kinetic energy cutoff for wave functions was 40 Ry and for the charge density and potential was 900 Ry. We also considered a Marzari-Vanderbilt smearing[20] with a Gaussian spreading of 10^{-8} Ry (except for the closed-shell solution of $P = 6$ that we employed Gaussian smearing with Gaussian spreading of 10^{-2} Ry because of convergence problems). Since we are assuming non-periodic systems, the lattice vectors were large enough to avoid interactions between the molecules. The magnetization consists in an integration of the magnetic density over a sphere of radius $R \approx 0.85$ a.u. around each atom. We also computed the periodic one-dimensional system, for which we kept the same convergence parameters as before, except a k-grid of $6 \times 1 \times 1$ and the lattice vector $|\vec{a}| = 14.6$ Å. For the case of the closed-shell solution, we needed a Gaussian smearing with Gaussian spreading of 0.02 Ry and a k-grid of $20 \times 1 \times 1$.

In addition, we repeated these calculations for the finite systems but changing the density functional and computational package. Specifically, we employed the PBE0 hybrid functional[21, 22] with the ORCA package[23, 24], with a def2-SVP basis[25], where the auxiliary basis set was automatically generated by the AutoAux keyword[26]. For the three considered systems, the FM dimers was the most stable solution. The relaxed geometry, as with QE, did not deviate from planarity. In Fig. S1 we show the local magnetic moments of the FM dimers, calculated with DFT.

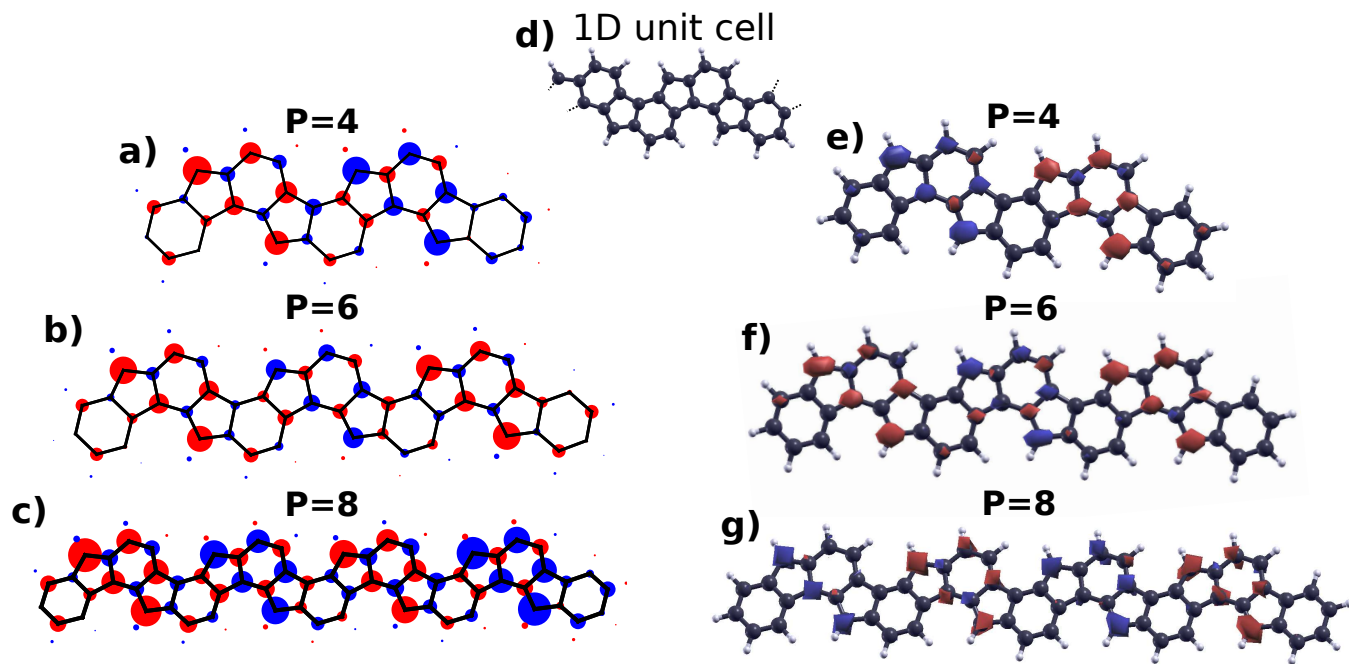


FIG. S1. Local magnetic moments per atom of the FM dimers solution calculated with DFT for isomer **1** molecules with $P = 4, 6$ and 8 , from top to bottom. Panels (a,b,c) are calculated with a PBE functional with QE, the highest local magnetic moment had $0.03\mu_B$, $0.07\mu_B$ and $0.05\mu_B$ for $P = 4, 6$ and 8 , respectively. d) Relaxed unit cell of the 1D periodic system, calculated with Quantum Espresso. Panels (e,f,g) are calculated with the PBE0 hybrid functional with ORCA and represented with a $0.01\mu_B/\text{\AA}^3$ isosurface.

II. MEAN-FIELD HUBBARD CALCULATIONS FOR ISOMERS **2**, **3**, **4**, **5** AND **6**

MF-Hubbard calculations carried on isomers **3**, **4**, **5** and **6** yield results in agreement with the analysis of magnetic interactions performed in this article (Fig. S2). The results for isomer **2**, as well as for a modified molecule in which the effective coupling between unpaired electrons is weakened by inserting a second hexagon between each pair of pentagons (Fig. S3), are explained in the main text. Some of these molecules show a spiral geometry for large enough systems. In our calculations here, we ignored the possible effects of this, preserving the single p_z orbital approximation with t first-neighbours hopping. Isomer **3** presents energy curves similar to that of isomer **1**, so the ferromagnetic dimers happen to be the lowest-energy solution for a range of U that is physically relevant, independently of the molecular length. Isomers **4**, **5** and **6** show antiferromagnetic order at the pentagon moments for a physically relevant range of U and for any length (Fig. S2). In the latter, however, $P = 2$ molecules are predicted to be closed-shell in the literature. MF-Hubbard calculations show that the U necessary to have magnetism decreases with P , so it would be in agreement with this.

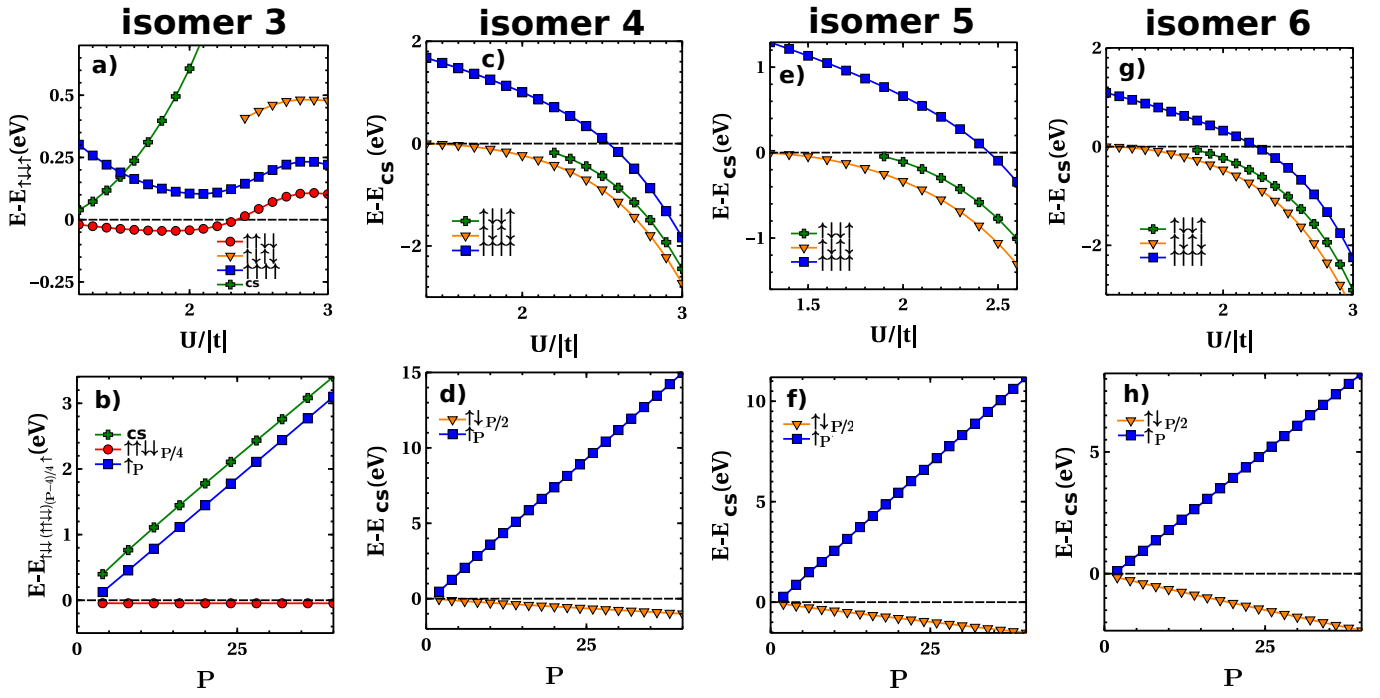


FIG. S2. MF-Hubbard calculations for isomers **3**, **4**, **5** and **6**. Top: Excitation energies as a function of U , with $P = 4$. Bottom: excitation energies as a function of the number of pentagons P with $U = 1.8|t|$. In all cases $t = -2.7$ eV.

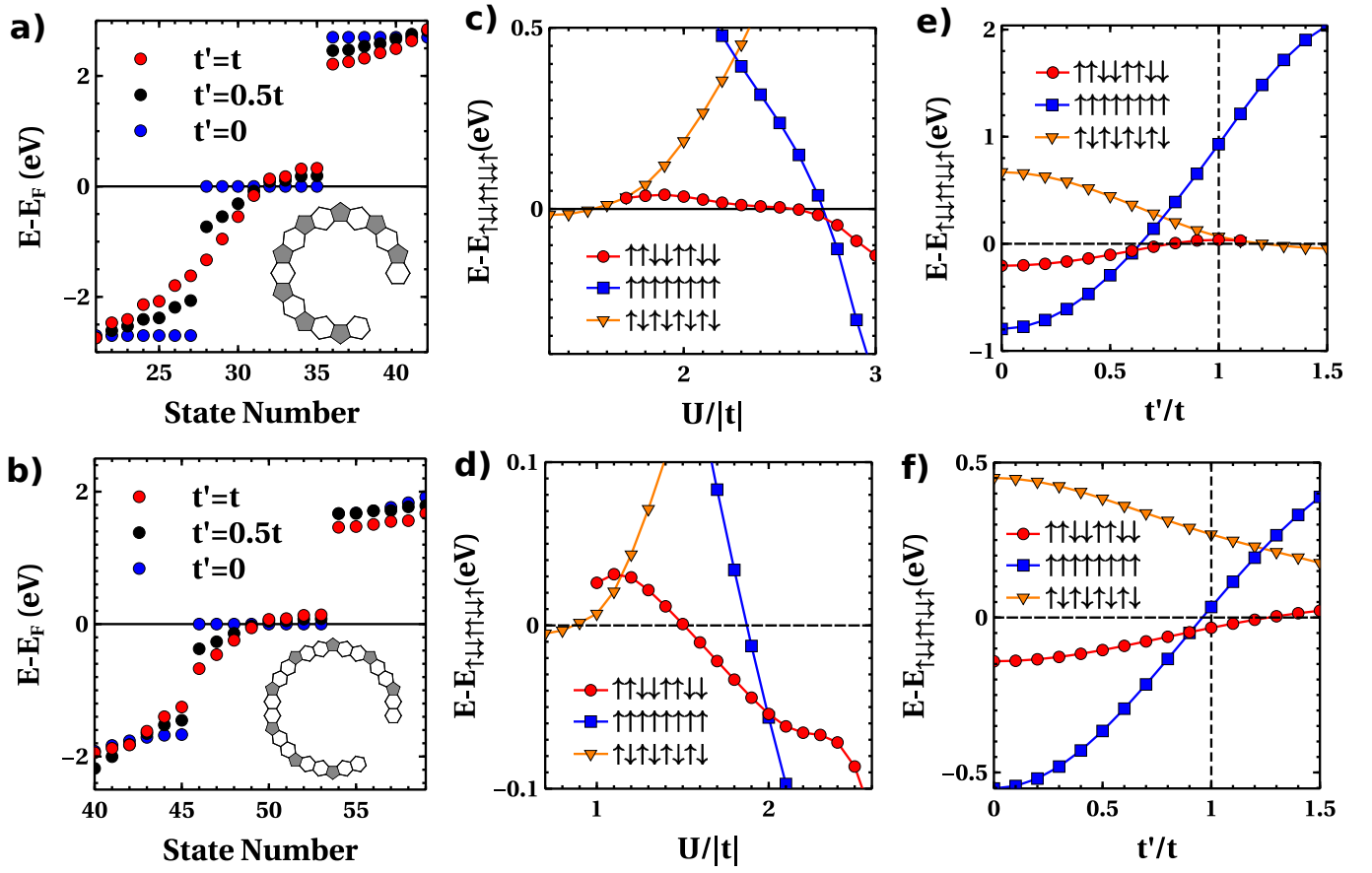


FIG. S3. (a), (b) Non-interacting spectra for different t' . (c), (d) Energy differences between different magnetic solutions as a function of U and $t' = t$, (e), (f) as a function of t' for $U = 1.8|t|$, calculated with MF-Hubbard. (a),(c),(e) are for a molecule of isomer **2** with $P = 8$ with one hexagon and (b),(d),(f) with two hexagons separating the pentagons (insets of (a),(b)).

III. CAS-HUBBARD CALCULATIONS

Additionally, we do a multiconfigurational calculation with CAS-Hubbard on isomers **1** and **2** (Figs. S4, S5, S6). Regarding isomer **1** with $P = 4$ ($P = 8$), we get an $S = 0$ ground state for $U < 4.3|t|$ ($U < 3.3|t|$), whilst for $U > 4.3|t|$ ($U > 3.3|t|$) the FM $S = 2$ ($S = 4$) solution becomes the lowest-energy state with CAS(8,8). For $P = 6$, we get an $S = 0$ ground state for $U < 0.8|t|$, whilst for $0.8|t| < U < 3.6|t|$ it is $S = 1$, and $S = 3$ for $U > 3.6|t|$. As it is explained in the manuscript, we ascribe the $S = 0$ ground state of $P = 4, 8$ molecules and the $S = 1$ ground state of the $P = 6$ molecule to a VBS. The $S = 0$ ground state for $P = 6$ at low U is consistent to a scenario where the FM first-neighbours exchange is still lower than the AF first-neighbours exchange. The FM ground state with $S = P/2$, that is seen for the three molecules when U is increased, would be in agreement with the expected behaviour of the frustrated FM spin chain. We include the spin correlators, calculated with the Hubbard model, for the $P = 4$ isomer **1** and the frustrated FM Heisenberg chain with four $S = 1/2$ spins (Fig. S4). They are in qualitative agreement, as it happens for the other lengths in the main text.

Here we also show a spin-correlator calculation for some isomer **2** molecules at $U = 1.5|t|$ (Fig. S6). As we show, the strength of the correlators alternate with the pair of adjacent pentagons, being negative in all cases. This is an indication of dimerization but with $S = 0$ for each dimer. As we mention in the main text, this is consistent with the frustrated AF spin model.

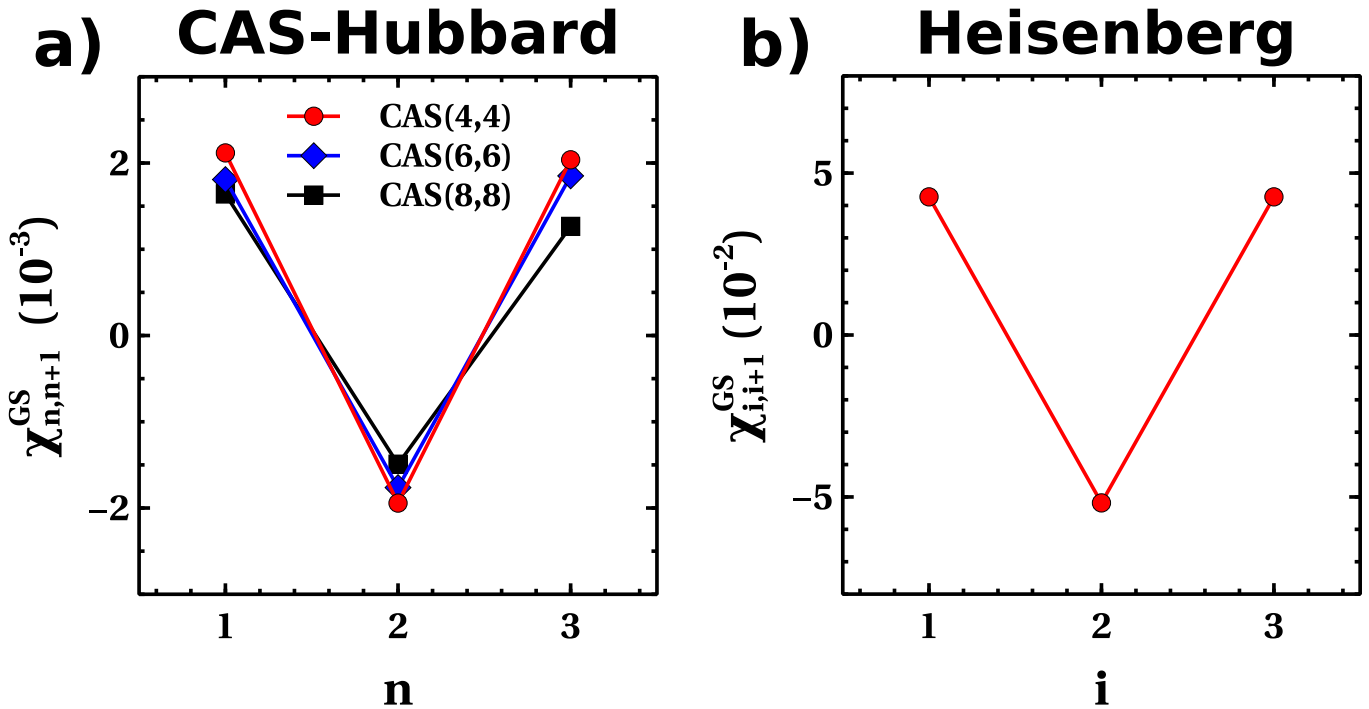


FIG. S4. a) Spin correlators for isomer **1** with $P = 4$, calculated with an exact diagonalization of the CAS-Hubbard model with $U = 1.5|t|$ and $t = -2.7$ eV. b) Spin correlators for the FM Heisenberg chain with second neighbours AF exchange and $J_1^{FM} = -2J_2^{AF}$.

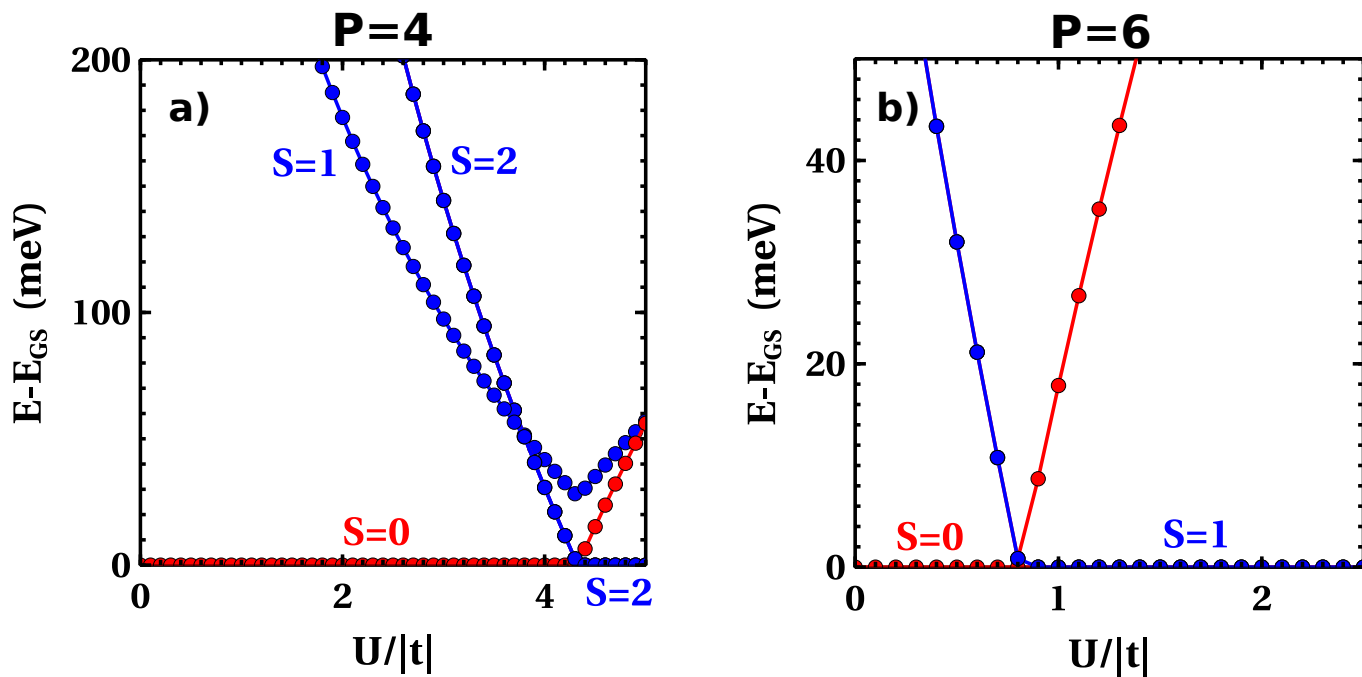


FIG. S5. Excitation energies for $P = 4, 6$ molecules of isomer 1, calculated with the CAS-Hubbard model with CAS(8,8), $t = -2.7$ eV.

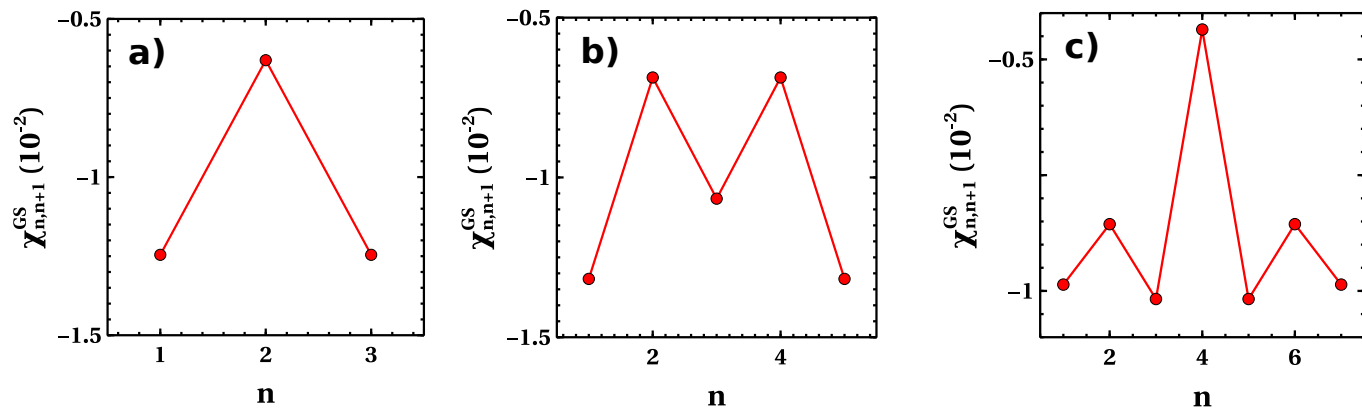


FIG. S6. Spin-correlators between the vertex carbons of adjacent pentagons of isomer 2 molecules with a) $P = 4$, b) $P = 6$ and c) $P = 8$, calculated with the CAS-Hubbard model with CAS(8,8), $t = -2.7$ eV and $U = 1.5|t|$. The ground state has $S = 0$.

IV. MAGNETIC INTERACTIONS ANALYSIS

It is possible to perform a similar analysis of the magnetic interactions as that of the main text but on the other isomers. In Fig. S7 we show this same analysis for the isomers **2** and **4**. As we can see, in isomer **2** we get the same kind of magnetic interactions as with isomer **1**, so it has competing AF and FM first-neighbours exchange and AF second-neighbours exchange. Isomer **4**, on the other hand, just presents first-neighbours AF exchange, so it has different physics. By doing the same analysis for the rest of the isomers, one gets that isomer **3** belongs to the class **I**, whilst isomers **5** and **6** belong to class **II** of OInIn.

For completeness, we want to go deeper with the idea that class **II** polymers are tight-binding chains. In Fig. S8 we show the non-interacting eigenvalues of a) a tight-binding chain with 16 sites, b) and c) $P = 16$ isomer **4** molecules with $t' = 0$ and $t' = t$, respectively. As we can see, at the spectrum of the molecule with $t' = 0$ the energy distribution of the states inside a gap and around the Fermi energy looks very similar to the tight-binding chain. When $t' = t$, the situation changes and the lower band gap closes by effect of t' , but the energy distribution still holds similarity. We also check this idea by comparing the wave functions of the first states around the Fermi energy (Fig. S9). For doing this, we employ a linear combination of pairs of states, that in the bipartite case present energies E and $-E$, and yield to sublattice polarized zero modes ($\psi_{L,R}^\delta = \psi_{HOMO+\delta} \pm \psi_{LUMO+\delta}$, where $\delta = 0, 1, 2, \dots$). As we can see, there is a strong correspondence between the probability distribution for the tight-binding chain and both $t' = 0$ and $t' = t$ molecules. In addition, we compute the tight-binding band structure of 1D isomer **4** systems, showing clearly a metallic behaviour, for both $t' = 0$ and $t' = t$, as it happens in the tight-binding chain (Fig. S10). These results are similar for isomers **5** and **6**.

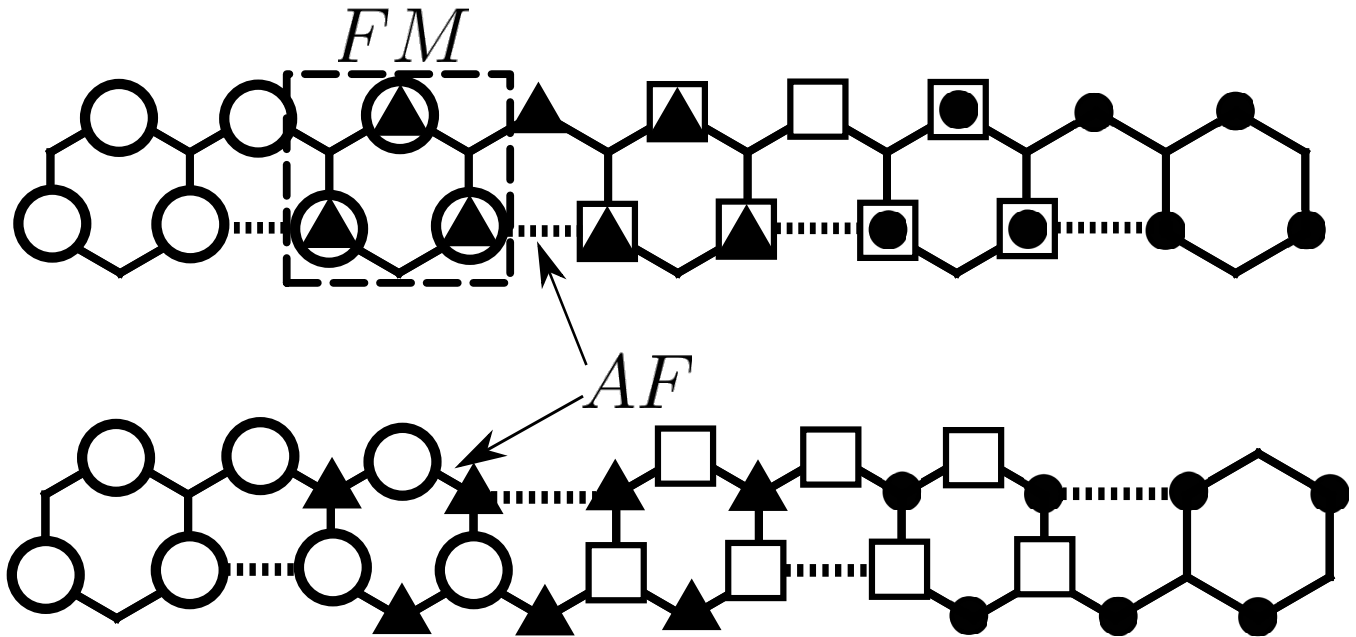


FIG. S7. Analysis of the magnetic interactions that are present in isomers **2** (top) and **4** (bottom).

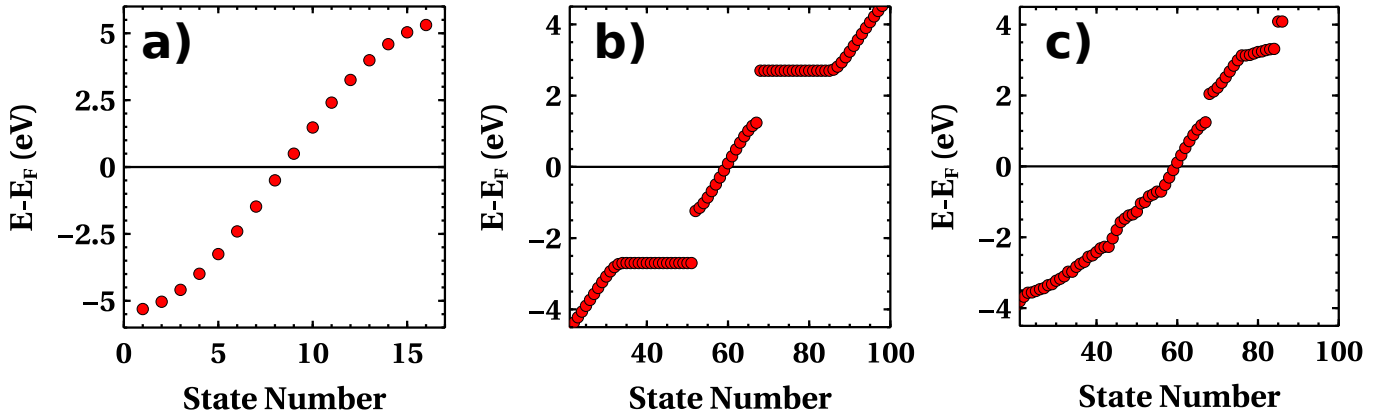


FIG. S8. Single-particle spectra, calculated with a tight-binding approximation with $t = -2.7$ eV, for a) a chain with 16 sites, b) an isomer 4 molecule with $P = 16$ and $t' = 0$, c) an isomer 4 molecule with $P = 16$ and $t' = t$.

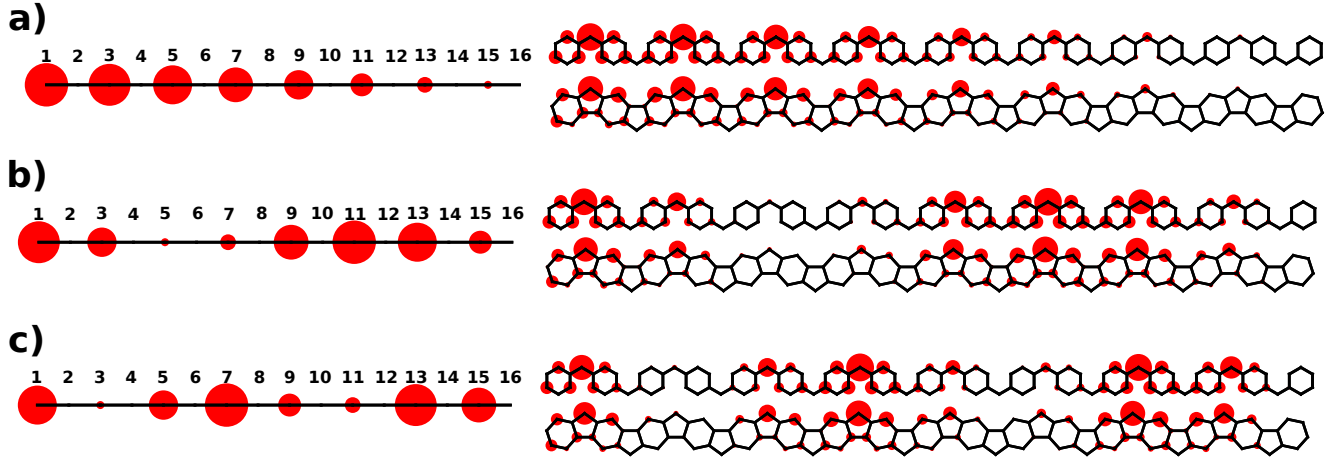


FIG. S9. Comparison of probability distribution of states that are linear combination of pairs of molecular orbitals around the Fermi energy. a) ψ_L^0 , b) ψ_L^1 and c) ψ_L^2 , respectively. This calculation is done for the three systems of Fig. S8.

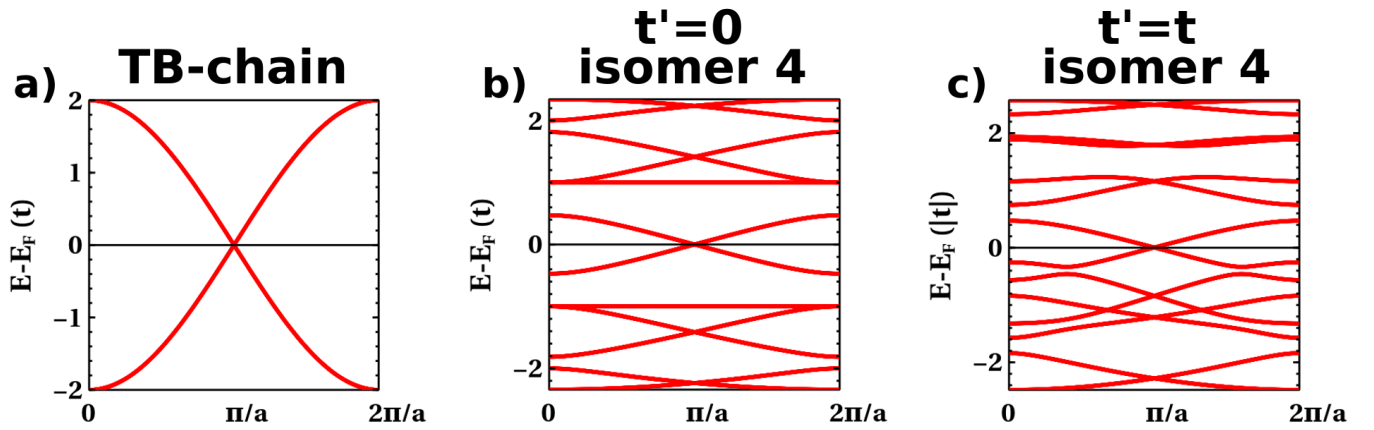


FIG. S10. Band structure for a one-dimensional system. a) tight-binding chain with two sites as unit cell, b) isomer 4 with $t' = 0$ and c) isomer 4 with $t' = t$.

-
- [1] S. Mishra, X. Yao, Q. Chen, K. Eimre, O. Gröning, R. Ortiz, M. Di-Giovannantonio, S.-G. J. Carlos, J. Fernández-Rossier, C. A. Pignedoli, K. Müllen, P. Ruffieux, A. Narita, and R. Fasel, Large magnetic exchange coupling in rhombus-shaped nanographenes with zigzag periphery, *Nat. Chem.* **13**, 581 (2021).
- [2] S. Mishra, D. Beyer, K. Eimre, R. Ortiz, J. Fernández-Rossier, R. Berger, O. Gröning, C. A. Pignedoli, R. Fasel, X. Feng, *et al.*, Collective all-carbon magnetism in triangulene dimers, *Angew. Chem. Int. Ed.* **59**, 12041 (2020).
- [3] S. Mishra, G. Catarina, F. Wu, R. Ortiz, D. Jacob, K. Eimre, J. Ma, C. A. Pignedoli, X. Feng, P. Ruffieux, *et al.*, Observation of fractional edge excitations in nanographene spin chains, *Nature* **598**, 287 (2021).
- [4] R. Ortiz, R. Á. Boto, N. García-Martínez, J. C. Sancho-García, M. Melle-Franco, and J. Fernández-Rossier, Exchange rules for diradical π -conjugated hydrocarbons, *Nano Lett.* **19**, 5991 (2019).
- [5] J. Fernández-Rossier and J. J. Palacios, Magnetism in graphene nanoislands, *Phys. Rev. Lett.* **99**, 177204 (2007).
- [6] J. Fernández-Rossier, Prediction of hidden multiferroic order in graphene zigzag ribbons, *Phys. Rev. B* **77**, 075430 (2008).
- [7] J. Lado, N. García-Martínez, and J. Fernández-Rossier, Edge states in graphene-like systems, *Synthetic Metals* **210**, 56 (2015), reviews of Current Advances in Graphene Science and Technology.
- [8] M. Fujita, K. Wakabayashi, K. Nakada, and K. Kusakabe, Peculiar localized state at zigzag graphite edge, *J. Phys. Soc. Jpn.* **65**, 1920 (1996).
- [9] K. Wakabayashi, M. Sigrist, and M. Fujita, Spin wave mode of edge-localized magnetic states in nanographite zigzag ribbons, *J. Phys. Soc. Jpn.* **67**, 2089 (1998).
- [10] F. Muñoz Rojas, J. Fernández-Rossier, and J. J. Palacios, Giant magnetoresistance in ultrasmall graphene based devices, *Phys. Rev. Lett.* **102**, 136810 (2009).
- [11] O. V. Yazyev, Emergence of magnetism in graphene materials and nanostructures, *Rep. Prog. Phys.* **73**, 056501 (2010).
- [12] O. V. Yazyev, R. B. Capaz, and S. G. Louie, Theory of magnetic edge states in chiral graphene nanoribbons, *Phys. Rev. B* **84**, 115406 (2011).
- [13] D. Soriano and J. Fernández-Rossier, Spontaneous persistent currents in a quantum spin hall insulator, *Phys. Rev. B* **82**, 161302 (2010).
- [14] Y. Shen and C.-F. Chen, Helicenes: synthesis and applications, *Chem. Rev.* **112**, 1463 (2012).
- [15] B. C. Baciú, T. de Ara, C. Sabater, C. Untiedt, and A. Guijarro, Helical nanostructures for organic electronics: the role of topological sulfur in ad hoc synthesized dithia[7]helicenes studied in the solid state and on a gold surface, *Nanoscale Adv.* **2**, 1921 (2020).
- [16] J. P. Perdew, K. Burke, and M. Ernzerhof, Generalized gradient approximation made simple, *Phys. Rev. Lett.* **77**, 3865 (1996).
- [17] P. Giannozzi, S. Baroni, N. Bonini, M. Calandra, R. Car, C. Cavazzoni, D. Ceresoli, G. L. Chiarotti, M. Cococcioni, I. Dabo, *et al.*, Quantum ESPRESSO: a modular and open-source software project for quantum simulations of materials, *J. Phys.: Condens. Matter* **21**, 395502 (2009).
- [18] P. Giannozzi, O. Andreussi, T. Brumme, O. Bunau, M. B. Nardelli, M. Calandra, R. Car, C. Cavazzoni, D. Ceresoli, M. Cococcioni, *et al.*, Advanced capabilities for materials modelling with Quantum ESPRESSO, *J. Phys.: Condens. Matter* **29**, 465901 (2017).
- [19] P. Giannozzi, O. Baseggio, P. Bonfà, D. Brunato, R. Car, I. Carnimeo, C. Cavazzoni, S. de Gironcoli, P. Delugas, F. Ferrari Ruffino, A. Ferretti, N. Marzari, I. Timrov, A. Urru, and S. Baroni, Quantum ESPRESSO toward the exascale, *J. Chem. Phys.* **152**, 154105 (2020).
- [20] N. Marzari, D. Vanderbilt, A. De Vita, and M. C. Payne, Thermal contraction and disordering of the al(110) surface, *Phys. Rev. Lett.* **82**, 3296 (1999).
- [21] J. P. Perdew, M. Ernzerhof, and K. Burke, Rationale for mixing exact exchange with density functional approximations, *J. Chem. Phys.* **105**, 9982 (1996).
- [22] C. Adamo and V. Barone, Toward reliable density functional methods without adjustable parameters: The pbe0 model, *J. Chem. Phys.* **110**, 6158 (1999).
- [23] F. Neese, The ORCA program system, *WIREs Computational Molecular Science* **2**, 73 (2012).
- [24] F. Neese, Definition of corresponding orbitals and the diradical character in broken symmetry dft calculations on spin coupled systems, *J. Phys. Chem. Solids* **65**, 781 (2004), design, Characterization and Modelling of Molecule-Based Magnetic Materials Proceedings of Symposium K, EMRS Spring Meeting, June 2003, Strasbourg, France.
- [25] F. Weigend and R. Ahlrichs, Balanced basis sets of split valence, triple zeta valence and quadruple zeta valence quality for H to Rn: Design and assessment of accuracy, *Phys. Chem. Chem. Phys.* **7**, 3297 (2005).
- [26] G. L. Stoychev, A. A. Auer, and F. Neese, Automatic generation of auxiliary basis sets, *J. Chem. Theory Comput.* **13**, 554 (2017).